Breast Cancer
Vol. 13 No. 1 January 2006

Review Article

Antitumor Protein Therapy; Application of the Protein Transduction Domain to the Development of a Protein Drug for Cancer Treatment

Hiroshi Harada*[1,2], Shinae Kizaka-Kondoh*[1,3], and Masahiro Hiraoka*[1]

*[1]*Department of Radiation Oncology and Image-applied Therapy, Kyoto University Graduate School of Medicine,* *[2]*Kyoto City Collaboration of Regional Entities for the Advancement of Technological Excellence, Japan Science and Technology Agency,* *[3]*COE formation for genomic analysis of disease model animals with multiple genetic alterations, Kyoto University Graduate School of Medicine, Japan.*

The genomic information obtained through the human genome project has been accelerating the analysis of the functions of various disease relevant genes. The high molecular weight biomolecules, including oligonucleotides, antisense nucleotides, small interference RNA and peptides, as well as genes (cDNA) and proteins, are becoming increasingly important for the development of molecular therapies. However, the potential of such information-rich macromolecules for therapeutic use has been limited by the poor permeability across the lipid bilayer of the cellular plasma membrane. Over the past decade, a unique activity of oligopeptides, known as protein transduction domains (PTDs) or cell penetrating peptides (CPPs), has made it possible to transduce biologically active macromolecules into living cells *in vitro* by conjugating a PTD to the desired macromolecule. Furthermore, this activity has also enabled the systemic delivery of bioactive macromolecules to all tissues in living animals. However, we are now confronted with the next difficulty delivering the macromolecules specifically to the therapeutic targets *in vivo*. In this review, we focus on the application of PTD to develop antitumor macromolecules and introduce several representative strategies to discriminate between tumor and normal tissue. In addition, we discuss the unique characteristics of breast cancer, which are expected to facilitate the application of PTD to develop novel protein therapy for breast cancer.

Breast Cancer 13:16-26, 2006.

Key words: Protein therapy, Protein transduction domain (PTD), HIV-1 tat, Tumor hypoxia, Hypoxia-inducible factor-1 (HIF-1)

Efficient internalization of therapeutic agents into target cells is critical to gain the desired therapeutic effect. However, since the plasma membrane of the cell surface forms an effective barrier and limits the internalization of high molecular weight materials into the cells, the application of information-rich macromolecules, such as DNA and proteins, to therapies has been restricted. A variety of methods have been widely proposed to effect their delivery into living cells *in vivo* as well as *in vitro*[1-3]; unfortunately, many of them have shown inefficient delivery. In these strategies, a number of other problems, such as complex manipulation, cellular toxicity and immunogenicity, have been reported and have prevented macromolecules from routine therapeutic use.

In 1988, Green *et al.* and Frankel *et al.* separately reported that the transcriptional activator of transcription (TAT) protein from human immunodeficiency virus-1 (HIV-1) has a unique potential to enter cells in culture when added exogenously[4,5]. The domain responsible for this translocation has been ascribed to the short basic region comprised by residues 47-57 of the TAT protein and is termed the "TAT protein transduction domain (PTD)"[6]. Subsequent studies have demon-

Reprint requests to Hiroshi Harada, Department of Radiation Oncology and Image-applied Therapy, Kyoto University Graduate School of Medicine, 54 Kawahara-cho, Shogoin, Sakyo-ku, Kyoto, 606-8507, Japan.
E-mail: hharada@kuhp.kyoto-u.ac.jp

Abbreviations:
PTD, Protein transduction domain; CPP, Cell penetrating peptide; HIF, Hypoxia-inducible factor; TAT, Transcriptional activator of transcription; HIV-1, Human immunodeficiency virus-1; IGF-I, Insulin-like growth factor-I; IGF-IR, IGF-I receptor; RCC, Renal cell carcinoma; VHL, Von Hippel-Lindau; CTL, Cytotoxic T lymphocyte; DC, Dendritic cell; OVA, Ovalbumin; TRP2, Tyrosinase-related protein 2; IAP, Inhibitors of apoptosis protein; Smac, Second mitochondria-derived activator of caspases; XIAP, X-linked IAP; TRAIL, Tumor necrosis factor-related apoptosis-inducing ligand; ODD, Oxygen-dependent degradation; β-Gal, β-galactosidase; TOP3, TAT-ODD-Procaspase-3; AI, Apoptosis index; pO_2, Oxygen partial pressure; RNAP, RNA polymerase

strated that TAT-PTD facilitates the internalization of conjugated proteins into living cells *in vitro*[6]. Likewise, a number of the other cationic peptides, e.g. the peptides from the third α helix of the antennapedia homeodomain and from the VP22 protein of the herpes simplex virus, have been reported as PTDs showing the same attractive activity as TAT-PTD[7]. The common feature among these peptides is their highly cationic nature, which is due to their high proportion of basic amino acids, such as arginine and lysine residues[8]. Using these PTDs, various kinds of physiologically and therapeutically active macromolecules, such as peptides, proteins[9], oligo DNAs[10], super magnet beads[11], liposomes[1] and λ phages[12] have been successfully transduced into living cells. Intracellular delivery of these macromolecules modulates the functions of various genes related to the cell cycle[13] and apoptosis[14] *in vitro*. Moreover, Schwarze *et al.* demonstrated that intraperitoneal injection of a TAT-PTD-fused 120 kDa β-galactosidase (β-Gal) protein resulted in the delivery of the biologically active fusion protein to all tissues in mice, including the brain[15]. Their results opened a new possibility for the direct delivery of macromolecules into patients as protein therapy. Indeed, several groups, including ours, have applied this strategy to develop novel protein drugs to treat preclinical tumor-bearing animals[16-20].

In this review, we describe the properties and the potential of TAT-PTD as a carrier of information-rich macromolecules, and introduce representative research, in which TAT-PTD-mediated protein therapy showed significant antitumor effects with target-specificity, but without side effects. Furthermore, we discuss the possibilities of such protein therapy for breast cancer treatment.

Mechanism of TAT-PTD-Mediated Protein Transduction into Living Cells

Despite the distinctive potential of the TAT-PTD and the other arginine- and/or lysine-rich peptides as carriers of macromolecules, little is known about the mechanism involved in the cellular uptake of PTD-fused macromolecules as well as the wild type HIV-1 TAT protein.

In the early days, it was reported that no inhibition of internalization was observed at 4 ℃[21], and similar observations were reported for the basic amino acid-rich peptide derived from the antennapedia homeodomain[22]. Therefore, until recently, it was widely assumed that the PTD-mediated internalization of macromolecules occurs in an energy- and receptor-independent manner and is alternatively based on direct transport through the lipid bilayer[21]. However, it has been reported that the energy- and receptor-independence of PTD-mediated internalization are due to experimental artifacts in the process of cell fixation prior to microscopic observation and also due to the inadequate removal of proteins bound to the cell surface[23, 24]. Furthermore, it has been reported that the internalization is almost completely suppressed at 4 ℃ in unfixed conditions[24, 25]. These results, together with the observation that heparan sulfate and the inhibitor of low density lipoprotein receptor-related protein precluded the cellular uptake of PTD-fused macromolecules[25, 26], suggest that the interaction of TAT-PTD with cell surface constituents plays an important role, and is followed by an active endocytic process. Several recent papers support the involvement of an endocytic pathway in the PTD-mediated protein internalization[27, 28].

Since endocytosis is a complex mechanism including several different pathways, the identification of the critical pathway responsible for the internalization has recently been commenced. Using a permeable TAT-Cre recombinase reporter assay on living cells, Wadia *et al.* extensively analyzed the mechanism of cellular uptake of TAT-fusion protein and clearly summarized the details in 2004. After the initial ionic cell-surface interaction, TAT-fusion proteins are rapidly internalized by lipid raft-dependent macropinocytosis, but are independent of interleukin-2 receptor/raft- caveolar- and clathrin-mediated endocytosis and phagocytosis[29]. On the other hand, Richard *et al.* demonstrated in 2005 that a specific inhibitor of clathrin-dependent endocytosis partially inhibits TAT peptide uptake, implicating this pathway in TAT-peptide entry[30]. The molecular basis for the PTD-mediated cellular uptake of macromolecules into living cells still remains controversial, so further study is necessary to fully understand the process.

Development of TAT-PTD-Mediated Antitumor Protein Therapies

Research on protein transduction has dramatically expanded from *in vitro* to *in vivo* in the last decade. The advantage of this application is that we can accomplish rapid and equal distribution of PTD-linked macromolecules to all tissues and

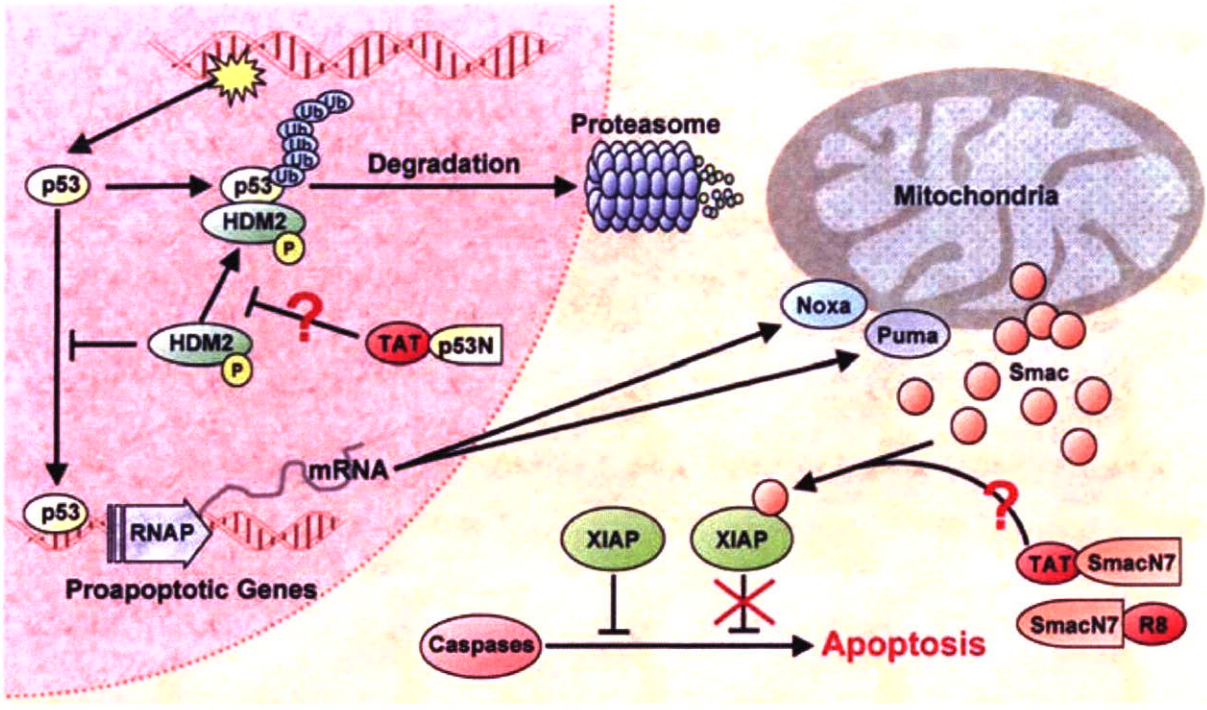

Fig 1. p53-related cellular apoptosis. HDM2 facilitates the proteolytic degradation of p53 protein. However, once damages of genomic DNA become severe, p53 is stabilized and induces various gene expressions such as Noxa and Puma and induce the release of Smac protein from mitochondria. The Smac protein interacts with XIAP and suppresses its activity, resulting in apoptosis. Since overexpression of HDM2 and IAPs inhibits apoptosis in many clinical tumors, the inhibition of their activities by p53N peptide and SmacN7 peptide respectively have been examined as novel antitumor strategies.

cells *in vivo*. However, it conversely leads to disadvantages in others. Especially for the development of PTD-fused anticancer macromolecules, the medications should have target-specificity and act locally, otherwise it may lead to damage of normal tissues and result in side effects. In the following sections, we describe representative applications showing target-specificity as well as the antitumor effect of TAT-mediated protein therapies *in vivo*.

1) Application of a Tumor Suppressor Gene, p53

Accumulated knowledge about signal cascades in cancer cells has revealed that genetic alterations of oncogenes and/or tumor suppressor genes make cells more malignant, resulting in deregulated proliferation and the evasion of apoptosis. In the development of novel cancer therapy, significant efforts at restoring the lesions that prevent the implementation of the apoptotic response have been made in order to specifically cause the death of malignant cells and in order to spare normal cells carrying few such apoptotic burdens. Such a strategy has been expected to show a much lower toxicity in normal tissue, compared with the conventional genotoxic agents that are currently in clinical use.

The gene encoding the tumor suppressor p53 is the most common anti-apoptotic lesion in cancer cells[31] and approximately 50% of human cancers bear p53 gene mutations. In most remaining cases, p53 activity is impaired by alternative molecular mechanisms, such as an elevated level of a p53 inhibitor, Mdm2[32] and the E6 protein of HPV[33], or silencing of a p53 co-activator, ARF[34, 35]. One of the most important functions of p53 is "cell cycle arrest", in which p53 disturbs the replication of damaged genomic DNA and the fixation of mutations, allowing for DNA repair. Another important function is the "induction of apoptosis", which occurs in cases in which the damage to the genomic DNA is too severe to be repaired (Fig 1). These abilities of p53 are essential for the proper regulation of cell proliferation in multi-cellular organisms[35]. Loss of these functions frequently leads to cellular neoplastic transformation, and increases the resistance of cancer cells to anti-cancer therapies[36]. Therefore, restoring p53 activity in tumor cells has been expected to be an effec-

tive strategy to induce cancer cell death in a large population of cancer patients. Gene therapy strategies have been indeed conducted to restore the tumor suppressor function of p53 with both viral and non-viral vectors. However, the efficacies of these approaches were difficult to confirm under certain conditions in clinical studies as well as in preclinical studies[37,38]. Some problems associated with immunogenicity and the low efficiency of systemic distribution were inevitable with this drug delivery system[39]. To overcome these difficulties, Tat-mediated approaches were carried out as follows.

Harbour *et al.* aimed to restore endogenous p53 activity by using a permeable peptide[18]. In the regulation of p53 activity, HDM2 interacts with the N-terminal region of the p53 protein and decreases the ability of p53 to act as a positive transcriptional factor and facilitates the proteolytic degradation of the p53 protein[40] (Fig 1). Indeed, the overexpression of HDM2 has been reported in many clinically recognized tumors, which contain the wild type p53 gene, and is associated with the functional inactivation of the p53 protein[41-43]. Therefore, it is anticipated that the disruption of the inhibitory effect of HDM2 on p53 activity would yield therapeutic benefits in tumor cells that over-express the HDM2 protein. To examine this hypothesis, the N-terminal region of the p53 protein was fused to the TAT-PTD. The resultant TAT-p53N peptide induced the rapid accumulation of p53 and the activation of apoptotic genes, and resulted in the preferential killing of tumor cells and the regression of human retinoblastoma cells in a rabbit eye[18]. Minimal retinal damage was observed after intravitreal injection[18].

2) Application of a Proapoptotic Gene, Smac

A major obstacle in cancer therapy is the resistance of cancer cells to current anticancer treatments, such as chemotherapy and radiotherapy[44]. Defects in apoptotic programs are caused by deregulated expression and function of the components of the apoptotic pathway and contribute to such resistance[45,46]. Inhibitors of apoptosis proteins (IAPs) are frequently overexpresssed in malignant tumors[47], and they inhibit caspase activity by directly binding to activated caspase-3 and-7[48,49]. The second mitochondria-derived activator of caspases (Smac) was identified as the protein that is released from the mitochondria to the cytosol in response to apoptotic stimuli and antagonizes IAPs to promote apoptosis[50,51] (Fig 1). Therefore, the up-regulation of Smac activity in tumor cells may improve the resistance to anticancer therapies (Fig 1).

Fulda *et al.* examined the hypothesis using cell-permeable synthetic Smac peptides (TAT-SmacN7 in this review) containing a polypeptide from the N-terminal of Smac protein for the inactivation of X-linked IAP (XIAP)[52,53]. As a result, the peptide enhanced the ability of Apo2L/tumor necrosis factor-related apoptosis-inducing ligand (TRAIL) in an intracranial malignant glioma xenograft model *in vivo*[52]. Moreover, the complete eradication of established tumors and the survival of mice were achieved only upon combined treatment with the Smac peptide and Apo2L/TRAIL. In these experiments, no detectable toxicity to normal brain tissue was observed.

Yang *et al.* examined whether the inhibition of IAPs combined with chemotherapy produced synergistic effects or not[19]. First of all, they confirmed that the defect in apoptosome activity was dramatically restored by the IAP-targeting SmacN7 peptide, which is the seven N-terminal amino residues of mature Smac and has the potential to disrupt XIAP-caspase-9 interaction. On the other hand, SmacN7 peptide did not show any striking effect on the apoptosome activity of normal lung fibroblast cells. They finally demonstrated that newly synthesized SmacN7 peptide fused to the cell membrane permeable polyarginine (SmacN7R8) strongly reversed the apoptosis resistance, and displayed a synergistic effect with chemotherapy *in vivo*.

3) Application of a Tumor Suppressor Gene, VHL

Since it was reported that the growths of a variety of cancer cells are dependent on insulin-like growth factor-I (IGF-I)-mediated signaling, inhibiting the pathway has shown therapeutic effects on a variety of experimental tumor xenografts (Fig 2). For example, a truncated form of the IGF-I receptor (IGF-IR) acts as a dominant negative inhibitor of IGF-IR and abrogates ligand-dependent cellular transformation and tumorigenesis *in vitro* and *in vivo*[54]. Similarly, a specific IGF-IR antibody[55] and a specific IGF-IR antisense oligonucleotide[56] suppress the tumor growth and prolong the survival of tumor-bearing mice, respectively. Renal cell carcinoma (RCC) was reported to be dependent on the IGF-I-mediated signaling pathway for its growth. Previously, Datta *et al.* reported that IGF-I-mediated signaling is inhibited in the

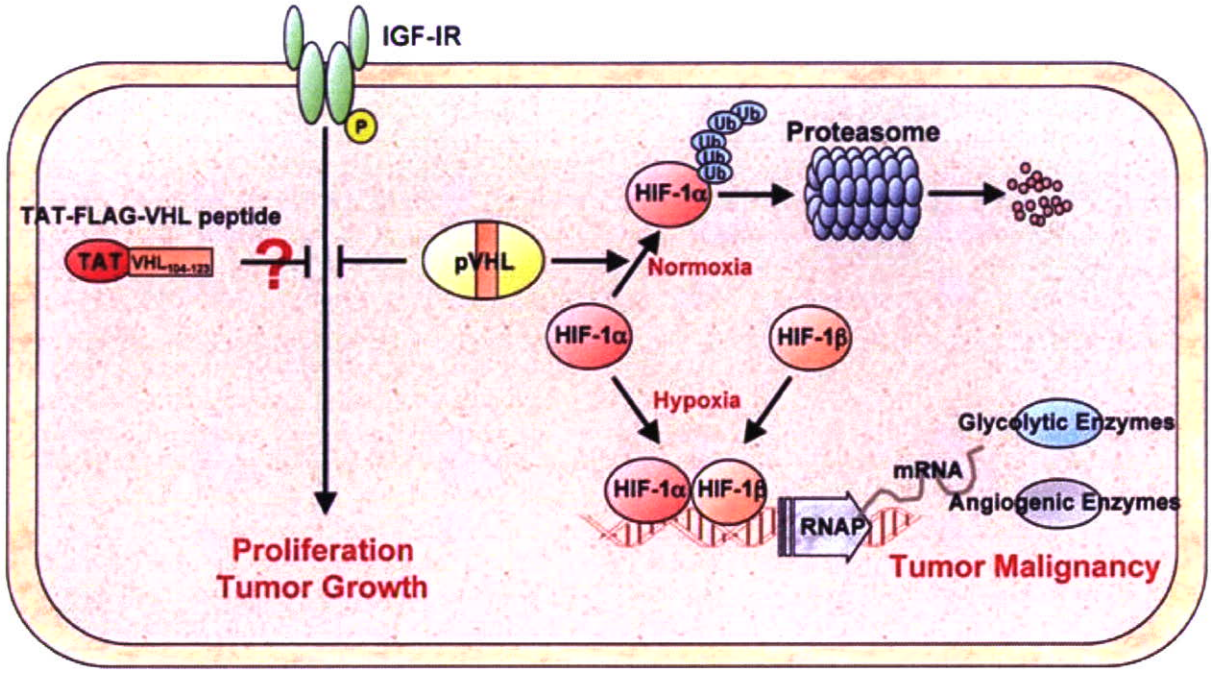

Fig 2. Function of pVHL in IGF-I-mediated signaling and in hypoxia-responsible gene expression. The growth of various cancer cells are dependent on IGF-I signaling. The signal is inhibited in the presence of pVHL in RCC cells, and thus inhibition of this signal pathway has been aimed by $VHL_{104\text{-}123}$ peptide. pVHL also acts on hypoxia-dependent gene expression. In normoxic conditions, hydroxylated HIF-1α protein is recognized by pVHL and ubiquitinated, resulting in the rapid proteolytic degradation. In hypoxic conditions, stabilized HIF-1α interacts with constitutively expressed HIF-1β and induces various gene expressions related to tumor malignancy.

presence of wild type von Hippel-Lindau tumor suppressor gene product (pVHL) in RCC cells and a specific amino acid sequence (104-123) in the β domain of the pVHL ($VHL_{104\text{-}123}$) is responsible for this function[57] (Fig 2). These results indicate that the pVHL function via the 104-123 amino acid region leads to the restricted IGF-IR signaling, resulting in restricted cell proliferation and restricted RCC growth. This is consistent with the reports that the VHL tumor suppressor gene is mutated in the majority of patients with RCCs, as well as in patients with VHL disease[58, 59], and that the mutations are located in one of the hotspots of the VHL gene[60]. In addition to a well-known function of pVHL to regulate the stability of hypoxia-inducible factor-1α (HIF-1α) protein[61], this activity must also play an important role in the tumorigenesis of RCCs.

Based on this preclinical research, Datta *et al.* examined the effects of $VHL_{104\text{-}123}$ on tumor characteristics[20] (Fig 2). $VHL_{104\text{-}123}$ conjugated to the TAT-PTD (TAT-FLAG-VHL peptide) inhibited the thymidine incorporation into RCC cells by nearly 80% compared with a counterpart protein (TAT-FLAG). Furthermore, the TAT-FLAG-VHL peptide inhibited the tyrosine phosphorylation of MAP kinase, an essential downstream molecule that leads to cell proliferation. Thus, these results suggest that TAT-FLAG-VHL peptide blocks the IGF-I-induced RCC proliferation *in vitro*. Furthermore, i.p. injection of TAT-FLAG-VHL peptide retarded the growth of subcutaneous RCC tumors, and in some cases, regressed the tumors volume, and dramatically inhibited the invasiveness deeper into the muscle layer.

4) Application of a HIF-1α ODD Domain; Development of Hypoxia-Targeting Protein Drug

The genetic alterations in tumor cells directly cause the deregulated proliferation and the high metabolic demands of tumor cells, which in turn lead to the development of hypoxia in solid tumors[62, 63]. Tumor hypoxia has been recognized as a tumor specific microenvironment, in other words, healthy adults probably have few such tissues. In such conditions, a transcriptional factor, hypoxia-inducible factor-1 (HIF-1), induces various genes related to angiogenesis[64] and glycolysis[65], and leads to invasive and metastatic properties in

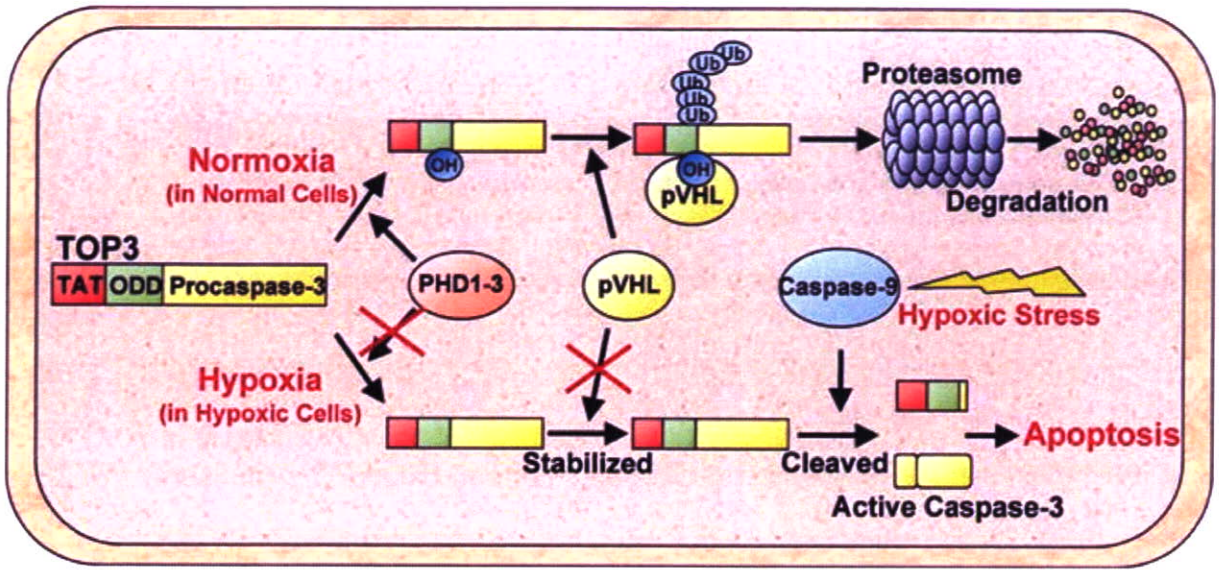

Fig 3. Hypoxia-dependent Proapoptotic Function of TOP3. TOP3 is degraded through the same ubiquitin-proteasome system as HIF-1α protein under normoxic conditions, but stabilized under hypoxic conditions. Because upstream caspases, *e.g.* caspases-9, are activated to some extent by hypoxic stress, TOP3 is cleaved to generate an active caspase-3, resulting in the enhancement of apoptotic cell death.

tumor cells[66]. HIF-1 activity is associated with the resistance of tumor cells to conventional radiotherapy and chemotherapy[67,68] and with the patient mortality in clinical studies[69-71]. Therefore, extensive efforts have been directed toward the development of novel therapies, which specifically damage the hypoxic/HIF-1-activating tumor cells[68,72].

HIF-1 is a heterodimeric transcriptional factor composed of an alpha subunit (HIF-1α) and a constitutively expressed beta subunit (HIF-1β)[73] (Fig 2). HIF-1α expression is tightly regulated at the post-translational level by oxygen-dependent prolyl hydroxylation and subsequent ubiquitination of its oxygen-dependent degradation (ODD) domain within the HIF-1α protein[61]. The pVHL is responsible for the ubiquitination. The stability of the HIF-1α protein is mainly responsible for the regulation of HIF-1 transcriptional activity[73].

We applied this unique property of the ODD domain to develop a novel hypoxia-targeting protein drug[16]. First of all, we identified the minimum region of the ODD domain responsible for the oxygen-dependent degradation of arbitrary proteins fused to it. As a result, we confirmed the hypoxia-dependent β-Gal and luciferase activity of ODD-β-Gal fusion protein[16] and ODD-Luciferase fusion protein (Harada *et al.*, in preparation), respectively, in the culture cell[16]. To apply the ODD-fusion protein to an *in vivo* study, we fused TAT-PTD to the N-terminal of the ODD-β-Gal protein and created a TAT-ODD-β-Gal triple fusion protein. After i.p. injection with the TAT-ODD-β-Gal fusion protein to subcutaneous tumor-bearing mice, the β-Gal activity and the existence of the fusion protein were detected only in the hypoxic regions of the solid tumor. On the other hand, they were not observed in the normal tissue. These results demonstrate that biologically active proteins can be exogenously delivered to hypoxic tumor cells by the TAT-ODD peptide *in vivo*. This was the first example demonstrating the target-specificity of TAT-mediated protein delivery. To examine whether the TAT-ODD fusion protein with cytotoxicity shows antitumor effects or not, the TAT-ODD peptide was further fused to a pro-apoptotic protein (Fig 3). We intentionally chose a precursor of caspase-3, procaspase-3, because it is activated in response to hypoxic stress, which was thought to reduce the possibility of side effects in the well-oxygenated normal tissues (Fig 3). Systemic administration with the resultant fusion protein, TAT-ODD-Procaspase-3 (TOP3), reduced the tumor mass as well as suppressed the tumor growth without any obvious side effects in tumor-bearing mice. The hypoxia-targeting effect of TOP3 was proven using a rat ascites model, in which intraperitoneal injection with MM1 cells results in highly hypoxic ascetic fluid[17]. Inoue *et*

al. demonstrated that intraperitoneal injection with TOP3 resulted in a significant increase in the lifespan of rats with the malignant ascites, and furthermore, 60% of the treated animals were cured without the recurrence of ascites.

5) Other Possibilities for the Development of TAT-PTD-Mediated Antitumor Protein Therapy

Several *in vitro* studies have reported other possibilities which may enable delivery of the biologically active macromolecule specifically to the desired tumor *in vivo*[74,75]. First, the fact that PTDs selectively interact with distinct glycosaminoglycan species may allow targeting of selective tissues that differ in their surface-expressed glycosaminoglycan patterns[27]. Second, by inserting a tissue- and organelle-specific cleavage recognition site between PTD and the macromolecule, PTD may be cleaved off, resulting in the accumulation of the PTD-free macromolecules in the desired tissue and organelle, respectively[76]. Third, it is also possible to generate a PTD-linked protein drug that specifically acts in tumor cells while not affecting normal cells, by applying transformed cell-specific protein activity[77]. Finally, by using a peptide that can be recognized by the tumor-specific membrane proteins, it may be possible to design a variety of proteins that specifically internalize into desired tissues.

Application of TAT-Mediated Protein Drugs to Breast Cancer Treatments

Low molecular weight chemical compounds easily pass through the cellular plasma membrane *in vitro*, and furthermore show efficient distribution *in vivo*, and thus they have been focused on for a long time in the development of anticancer drugs. Almost all of the conventional chemotherapeutic agents, however, show low target-specificity and largely affect normal tissues as well as tumors. TAT-PTD has also been reported to transduce various macromolecules to all tissues *in vivo*[15], so this technique may cause side effects, but for additional devices. Over the past decade, several modifications have been examined to achieve a tumor-specific antitumor effect of PTD-mediated strategies, as mentioned above. To apply TAT-mediated protein therapy to breast cancer treatments, it is necessary to understand the common features among breast cancers and utilize them to construct a protein drug targeting breast cancer. In the remainder of the present review, we will discuss the characteristics of breast cancer and the possibilities of PTD-mediated protein therapy targeting then.

Pusztai *et al.* identified a number of novel and routine prognostic markers of breast cancer by analyzing the gene expression profiles obtained from fine-needle aspirations of breast cancer[78]. From their list, we may be able to find a novel protein that is specifically stabilized in breast cancer, but degraded in normal tissues, and to apply such regulation to develop a breast cancer-targeting protein drug.

The role of apoptosis in oncogenesis is currently being studied intensively in breast cancer[79]. A decrease in the apoptosis index (AI) due to the overexpression of IAPs and the mutation of the p53 gene must lead to the resistance of cancer cells to current anticancer treatments, such as chemotherapy and radiotherapy[44]. Several studies have analyzed the prognostic significance of AI in breast carcinomas. Lipponen *et al.* showed a significant difference in survival from breast carcinoma ($n = 288$) depending on the AI value (cut-off point for AI was $10/mm^2$)[80,81]. Zhang *et al.* also reported a 30% difference in survival at 5 years ($p < 0.001$) in 126 patients with breast carcinoma (cut-off point for AI was $11/mm^2$)[82]. These reports indicate that the induction of apoptosis prolongs the survival of patients with breast carcinoma. In this sense, a protein, which has the potential to induce cellular apoptosis, may be a reliable candidate to be introduced into the breast carcinoma.

Chromosome 3P allele loss is a frequent event in a variety of common sporadic cancers, and breast carcinoma is no exception. To analyze the extent and frequency of 3p allelic losses in early stage invasive sporadic breast carcinoma, loss of heterozygosity analysis was carried out using a 3p microsatellite marker by Martinez *et al.*[83]. They reported that 6 out of 22 tumors showed loss at 3p25-24, including the von hippel landau locus. In such breast carcinomas, IGF-IR signaling must not be suppressed because of the VHL-deficiency, resulting in unrestricted cell proliferation. Therefore, the introduction of $VHL_{104\text{-}123}$ with TAT-PTD is expected to show an antitumor effect. Moreover, VHL-deficiency must lead to the stabilization of HIF-1α protein in such breast carcinomas. Since the stability of TOP3 is regulated by pVHL via the same ODD-regulation as the HIF-1α protein, TOP3 must be stabilized even in the aerobic regions of such breast cancers, as well as in the hypoxic regions. Therefore, we can expect addi-

tional efficacy of TOP3 toward this type of breast cancer.

The accessibility of breast carcinomas permits the use of a polarographic needle electrode to measure the oxygen tension directly in cancer patients. Such studies have shown a significantly lower median oxygen partial pressure (pO_2) in malignant tumors compared with benign tumors and normal breast tissue. The median pO_2 values in malignant tumors, in benign tumors and in normal tissues were in the range of 23-28 mmHg, 42 mmHg and 54-65 mmHg, respectively[84, 85]. Of all readings in breast cancers, 30-40% fell below 10 mmHg, which is uncommon in normal tissue. Forty % of breast carcinomas contain almost anoxic regions in the range 0-2.5 mmHg, in which tumor cells still survive[84]. In such a microenvironment, the expression of the HIF-1α protein is usually induced. Bos *et al.* reported that HIF-1α proteins were indeed accumulated in breast cancers, and furthermore, the frequency of HIF-1α-positive cells increased in parallel with the increasing pathological stage of each sample[86]. Therefore, the novel hypoxia-targeting protein drug, TOP3, will likely show antitumor effects on malignant breast cancer.

Distribution of chemotherapeutic agents from tumor blood vessels to hypoxic tumor cells is also limited and thus only poor efficacy is usually obtained in conventional cancer chemotherapy. On the other hand, biologically active proteins could be delivered into whole tumor including hypoxic tumor cells, after i.p. injection with the fusion protein genetically conjugated with TAT-PTD[16]. This result demonstrates that TAT-PTD solves the problem of the poor delivery of anticancer agents to hypoxic tumor cells. Therefore, we can expect further effects of TOP3 on hypoxic cells in breast cancer.

Acknowledgements

This work was supported by a Grant-in-Aid for Kyoto City Collaboration of Regional Entities for the Advancement of Technological Excellence from Japan Science and Technology Agency, and by a Grant-in-Aid for Cancer Research from the Ministry of Education, Culture, Sports, Science and Technology, and by a Grant-in-Aid for the 2nd Term Comprehensive 10-Year Strategy for Cancer Control from the Ministry of Health, Labour and Welfare, Japan.

References

1) Torchilin VP, Rammohan R, Weissig V, Levchenko TS: TAT peptide on the surface of liposomes affords their efficient intracellular delivery even at low temperature and in the presence of metabolic inhibitors. *Proc Natl Acad Sci USA* 98:8786-8791, 2001.
2) Yamada T, Iwasaki Y, Tada H, Iwabuki H, Chuah MK, VandenDriessche T, Fukuda H, Kondo A, Ueda M, Seno M, Tanizawa K, Kuroda S: Nanoparticles for the delivery of genes and drugs to human hepatocytes. *Nat Biotechnol* 21:885-890, 2003.
3) Qian ZM, Li H, Sun H, Ho K: Targeted drug delivery via the transferrin receptor-mediated endocytosis pathway. *Pharmacol Rev* 54:561-587, 2002.
4) Green M, Loewenstein PM: Autonomous functional domains of chemically synthesized human immunodeficiency virus tat trans-activator protein. *Cell* 55:1179-1188, 1988.
5) Frankel AD, Pabo CO: Cellular uptake of the tat protein from human immunodeficiency virus. *Cell* 55:1189-1193, 1988.
6) Becker-Hapak M, McAllister SS, Dowdy SF: TAT-mediated protein transduction into mammalian cells. *Methods* 24:247-256, 2001.
7) Jarver P, Langel U: The use of cell-penetrating peptides as a tool for gene regulation. *Drug Discov Today* 9:395-402, 2004.
8) Futaki S: Membrane-permeable arginine-rich peptides and the translocation mechanisms. *Adv Drug Deliv Rev* 57:547-558, 2005.
9) Fawell S, Seery J, Daikh Y, Moore C, Chen LL, Pepinsky B, Barsoum J: Tat-mediated delivery of heterologous proteins into cells. *Proc Natl Acad Sci USA* 91:664-668, 1994.
10) Astriab-Fisher A, Sergueev DS, Fisher M, Shaw BR, Juliano RL: Antisense inhibition of P-glycoprotein expression using peptide-oligonucleotide conjugates. *Biochem Pharmacol* 60:83-90, 2000.
11) Lewin M, Carlesso N, Tung CH, Tang XW, Cory D, Scadden DT, Weissleder R: Tat peptide-derivatized magnetic nanoparticles allow in vivo tracking and recovery of progenitor cells. *Nat Biotechnol* 18:410-414, 2000.
12) Eguchi A, Akuta T, Okuyama H, Senda T, Yokoi H, Inokuchi H, Fujita S, Hayakawa T, Takeda K, Hasegawa M, Nakanishi M: Protein transduction domain of HIV-1 Tat protein promotes efficient delivery of DNA into mammalian cells. *J Biol Chem* 276:26204-26210, 2001.
13) Ezhevsky SA, Nagahara H, Vocero-Akbani AM, Gius DR, Wei MC, Dowdy SF: Hypo-phosphorylation of the retinoblastoma protein (pRb) by cyclin D:Cdk4/6 complexes results in active pRb. *Proc Natl Acad Sci USA* 94:10699-10704, 1997.
14) Troy CM, Stefanis L, Prochiantz A, Greene LA, Shelanski ML: The contrasting roles of ICE family proteases and interleukin-1beta in apoptosis induced by trophic factor withdrawal and by copper/zinc superoxide dismutase down-regulation. *Proc Natl Acad Sci USA* 93:5635-5640, 1996.
15) Schwarze SR, Ho A, Vocero-Akbani A, Dowdy SF: In vivo protein transduction: delivery of a biologically active protein into the mouse. *Science* 285:1569-1572,

1999.
16) Harada H, Hiraoka M, Kizaka-Kondoh S: Antitumor effect of TAT-oxygen-dependent degradation-caspase-3 fusion protein specifically stabilized and activated in hypoxic tumor cells. *Cancer Res* 62:2013-2018, 2002.
17) Inoue M, Mukai M, Hamanaka Y, Tatsuta M, Hiraoka M, Kizaka-Kondoh S: Targeting hypoxic cancer cells with a protein prodrug is effective in experimental malignant ascites. *Int J Oncol* 25:713-720, 2004.
18) Harbour JW, Worley L, Ma D, Cohen M: Transducible peptide therapy for uveal melanoma and retinoblastoma. *Arch Ophthalmol* 120:1341-1346, 2002.
19) Yang L, Mashima T, Sato S, Mochizuki M, Sakamoto H, Yamori T, Oh-Hara T, Tsuruo T: Predominant suppression of apoptosome by inhibitor of apoptosis protein in non-small cell lung cancer H460 cells: therapeutic effect of a novel polyarginine-conjugated Smac peptide. *Cancer Res* 63:831-837, 2003.
20) Datta K, Sundberg C, Karumanchi SA, Mukhopadhyay D: The 104-123 amino acid sequence of the beta-domain of von Hippel-Lindau gene product is sufficient to inhibit renal tumor growth and invasion. *Cancer Res* 61:1768-1775, 2001.
21) Vives E, Brodin P, Lebleu B: A truncated HIV-1 Tat protein basic domain rapidly translocates through the plasma membrane and accumulates in the cell nucleus. *J Biol Chem* 272:16010-16017, 1997.
22) Derossi D, Calvet S, Trembleau A, Brunissen A, Chassaing G, Prochiantz A: Cell internalization of the third helix of the Antennapedia homeodomain is receptor-independent. *J Biol Chem* 271:18188-18193, 1996.
23) Lundberg M, Wikstrom S, Johansson M: Cell surface adherence and endocytosis of protein transduction domains. *Mol Ther* 8:143-150, 2003.
24) Richard JP, Melikov K, Vives E, Ramos C, Verbeure B, Gait MJ, Chernomordik LV, Lebleu B: Cell-penetrating peptides. A reevaluation of the mechanism of cellular uptake. *J Biol Chem* 278:585-590, 2003.
25) Liu Y, Jones M, Hingtgen CM, Bu G, Laribee N, Tanzi RE, Moir RD, Nath A, He JJ: Uptake of HIV-1 tat protein mediated by low-density lipoprotein receptor-related protein disrupts the neuronal metabolic balance of the receptor ligands. *Nat Med* 6:1380-1387, 2000.
26) Tyagi M, Rusnati M, Presta M, Giacca M: Internalization of HIV-1 tat requires cell surface heparan sulfate proteoglycans. *J Biol Chem* 276:3254-3261, 2001.
27) Console S, Marty C, Garcia-Echeverria C, Schwendener R, Ballmer-Hofer K: Antennapedia and HIV transactivator of transcription (TAT) "protein transduction domains" promote endocytosis of high molecular weight cargo upon binding to cell surface glycosaminoglycans. *J Biol Chem* 278:35109-35114, 2003.
28) Fittipaldi A, Ferrari A, Zoppe M, Arcangeli C, Pellegrini V, Beltram F, Giacca M: Cell membrane lipid rafts mediate caveolar endocytosis of HIV-1 Tat fusion proteins. *J Biol Chem* 278:34141-34149, 2003.
29) Wadia JS, Stan RV, Dowdy SF: Transducible TAT-HA fusogenic peptide enhances escape of TAT-fusion proteins after lipid raft macropinocytosis. *Nat Med* 10:310-315, 2004.
30) Richard JP, Melikov K, Brooks H, Prevot P, Lebleu B, Chernomordik LV: Cellular Uptake of Unconjugated TAT Peptide Involves Clathrin-dependent Endocytosis and Heparan Sulfate Receptors. *J Biol Chem* 280:15300-15306, 2005.
31) Vousden KH, Lu X: Live or let die: the cell's response to p53. *Nat Rev Cancer* 2:594-604, 2002.
32) Momand J, Zambetti GP, Olson DC, George D, Levine AJ: The mdm-2 oncogene product forms a complex with the p53 protein and inhibits p53-mediated transactivation. *Cell* 69:1237-1245, 1992.
33) Scheffner M, Werness BA, Huibregtse JM, Levine AJ, Howley PM: The E6 oncoprotein encoded by human papillomavirus types 16 and 18 promotes the degradation of p53. *Cell* 63:1129-1136, 1990.
34) Kamijo T, Weber JD, Zambetti G, Zindy F, Roussel MF, Sherr CJ: Functional and physical interactions of the ARF tumor suppressor with p53 and Mdm2. *Proc Natl Acad Sci USA* 95:8292-8297, 1998.
35) Vogelstein B, Lane D, Levine AJ: Surfing the p53 network. *Nature* 408:307-310, 2000.
36) Sherr CJ, McCormick F: The RB and p53 pathways in cancer. *Cancer Cell* 2:103-112, 2002.
37) Roth JA, Nguyen D, Lawrence DD, Kemp BL, Carrasco CH, Ferson DZ, Hong WK, Komaki R, Lee JJ, Nesbitt JC, Pisters KM, Putnam JB, Schea R, Shin DM, Walsh GL, Dolormente MM, Han CI, Martin FD, Yen N, Xu K, Stephens LC, McDonnell TJ, Mukhopadhyay T, Cai D: Retrovirus-mediated wild-type p53 gene transfer to tumors of patients with lung cancer. *Nat Med* 2:985-991, 1996.
38) Seth P, Katayose D, Li Z, Kim M, Wersto R, Craig C, Shanmugam N, Ohri E, Mudahar B, Rakkar AN, Kodali P, Cowan K: A recombinant adenovirus expressing wild type p53 induces apoptosis in drug-resistant human breast cancer cells: a gene therapy approach for drug-resistant cancers. *Cancer Gene Ther* 4:383-390, 1997.
39) McCormick F: Cancer gene therapy: fringe or cutting edge? *Nat Rev Cancer* 1:130-141, 2001.
40) Wu X, Bayle JH, Olson D, Levine AJ: The p53-mdm-2 autoregulatory feedback loop. *Genes Dev* 7:1126-1132, 1993.
41) Polsky D, Melzer K, Hazan C, Panageas KS, Busam K, Drobnjak M, Kamino H, Spira JG, Kopf AW, Houghton A, Cordon-Cardo C, Osman I: HDM2 protein overexpression and prognosis in primary malignant melanoma. *J Natl Cancer Inst* 94:1803-1806, 2002.
42) Mori S, Ito G, Usami N, Yoshioka H, Ueda Y, Kodama Y, Takahashi M, Fong KM, Shimokata K, Sekido Y: p53 apoptotic pathway molecules are frequently and simultaneously altered in nonsmall cell lung carcinoma. *Cancer* 100:1673-1682, 2004.
43) Berger AJ, Camp RL, Divito KA, Kluger HM, Halaban R, Rimm DL: Automated quantitative analysis of HDM2 expression in malignant melanoma shows association with early-stage disease and improved outcome. *Cancer Res* 64:8767-8772, 2004.
44) Lowe SW, Lin AW: Apoptosis in cancer. *Carcinogenesis* 21:485-495, 2000.
45) Goyal L: Cell death inhibition: keeping caspases in check. *Cell* 104:805-808, 2001.
46) Deveraux QL, Reed JC: IAP family proteins–suppressors of apoptosis. *Genes Dev* 13:239-252, 1999.
47) Nachmias B, Ashhab Y, Ben-Yehuda D: The inhibitor of apoptosis protein family (IAPs): an emerging therapeutic target in cancer. *Semin Cancer Biol* 14:231-243, 2004.
48) Deveraux QL, Takahashi R, Salvesen GS, Reed JC: X-linked IAP is a direct inhibitor of cell-death proteases.

Nature 388:300-304, 1997.
49) Roy N, Deveraux QL, Takahashi R, Salvesen GS, Reed JC: The c-IAP-1 and c-IAP-2 proteins are direct inhibitors of specific caspases. *EMBO J* 16:6914-6925, 1997.
50) Du C, Fang M, Li Y, Li L, Wang X: Smac, a mitochondrial protein that promotes cytochrome c-dependent caspase activation by eliminating IAP inhibition. *Cell* 102:33-42, 2000.
51) Verhagen AM, Ekert PG, Pakusch M, Silke J, Connolly LM, Reid GE, Moritz RL, Simpson RJ, Vaux DL: Identification of DIABLO, a mammalian protein that promotes apoptosis by binding to and antagonizing IAP proteins. *Cell* 102:43-53, 2000.
52) Fulda S, Wick W, Weller M, Debatin KM: Smac agonists sensitize for Apo2L/TRAIL- or anticancer drug-induced apoptosis and induce regression of malignant glioma in vivo. *Nat Med* 8:808-815, 2002.
53) Wu G, Chai J, Suber TL, Wu JW, Du C, Wang X, Shi Y: Structural basis of IAP recognition by Smac/DIABLO. *Nature* 408:1008-1012, 2000.
54) Prager D, Li HL, Asa S, Melmed S: Dominant negative inhibition of tumorigenesis in vivo by human insulin-like growth factor I receptor mutant. *Proc Natl Acad Sci USA* 91:2181-2185, 1994.
55) Kalebic T, Tsokos M, Helman LJ: In vivo treatment with antibody against IGF-1 receptor suppresses growth of human rhabdomyosarcoma and down-regulates p34cdc2. *Cancer Res* 54:5531-5534, 1994.
56) Lee CT, Wu S, Gabrilovich D, Chen H, Nadaf-Rahrov S, Ciernik IF, Carbone DP: Antitumor effects of an adenovirus expressing antisense insulin-like growth factor I receptor on human lung cancer cell lines. *Cancer Res* 56:3038-3041, 1996.
57) Datta K, Nambudripad R, Pal S, Zhou M, Cohen HT, Mukhopadhyay D: Inhibition of insulin-like growth factor-I-mediated cell signaling by the von Hippel-Lindau gene product in renal cancer. *J Biol Chem* 275:20700-20706, 2000.
58) Gnarra JR, Tory K, Weng Y, Schmidt L, Wei MH, Li H, Latif F, Liu S, Chen F, Duh FM, Lubensky I, Duan DR, Florence C, Pzzatti R, Walther MM, Bander NH, Grossman HB, Brauch H, Pomer S, Brooks JD, Isaacs WB, Lerman MI, Zbar B, Linehan WM: Mutations of the VHL tumour suppressor gene in renal carcinoma. *Nat Genet* 7:85-90, 1994.
59) Shuin T, Kondo K, Torigoe S, Kishida T, Kubota Y, Hosaka M, Nagashima Y, Kitamura H, Latif F, Zbar B, *et al*: Frequent somatic mutations and loss of heterozygosity of the von Hippel-Lindau tumor suppressor gene in primary human renal cell carcinomas. *Cancer Res* 54:2852-2855, 1994.
60) Olschwang S, Richard S, Boisson C, Giraud S, Laurent-Puig P, Resche F, Thomas G: Germline mutation profile of the VHL gene in von Hippel-Lindau disease and in sporadic hemangioblastoma. *Hum Mutat* 12:424-430, 1998.
61) Semenza GL: HIF-1, O(2), and the 3 PHDs: how animal cells signal hypoxia to the nucleus. *Cell* 107:1-3, 2001.
62) Vaupel P, Kallinowski F, Okunieff P: Blood flow, oxygen and nutrient supply, and metabolic microenvironment of human tumors: a review. *Cancer Res* 49:6449-6465, 1989.
63) Dang CV, Semenza GL: Oncogenic alterations of metabolism. *Trends Biochem Sci* 24:68-72, 1999.
64) Forsythe JA, Jiang BH, Iyer NV, Agani F, Leung SW, Koos RD, Semenza GL: Activation of vascular endothelial growth factor gene transcription by hypoxia-inducible factor 1. *Mol Cell Biol* 16:4604-4613, 1996.
65) Semenza GL, Roth PH, Fang HM, Wang GL: Transcriptional regulation of genes encoding glycolytic enzymes by hypoxia-inducible factor 1. *J Biol Chem* 269:23757-23763, 1994.
66) Zhong H, De Marzo AM, Laughner E, Lim M, Hilton DA, Zagzag D, Buechler P, Isaacs WB, Semenza GL, Simons JW: Overexpression of hypoxia-inducible factor 1alpha in common human cancers and their metastases. *Cancer Res* 59:5830-5835, 1999.
67) Brown JM: The hypoxic cell: a target for selective cancer therapy–eighteenth Bruce F. Cain Memorial Award lecture. *Cancer Res* 59:5863-5870, 1999.
68) Semenza GL: Targeting HIF-1 for cancer therapy. *Nat Rev Cancer* 3:721-732, 2003.
69) Birner P, Gatterbauer B, Oberhuber G, Schindl M, Rossler K, Prodinger A, Budka H, Hainfellner JA: Expression of hypoxia-inducible factor-1 alpha in oligodendrogliomas: its impact on prognosis and on neoangiogenesis. *Cancer* 92:165-171, 2001.
70) Schindl M, Schoppmann SF, Samonigg H, Hausmaninger H, Kwasny W, Gnant M, Jakesz R, Kubista E, Birner P, Oberhuber G; Austrian Breast and Colorectal Cancer Study Group: Overexpression of hypoxia-inducible factor 1alpha is associated with an unfavorable prognosis in lymph node-positive breast cancer. *Clin Cancer Res* 8:1831-1837, 2002.
71) Birner P, Schindl M, Obermair A, Plank C, Breitenecker G, Oberhuber G: Overexpression of hypoxia-inducible factor 1alpha is a marker for an unfavorable prognosis in early-stage invasive cervical cancer. *Cancer Res* 60:4693-4696, 2000.
72) Kizaka-Kondoh S, Inoue M, Harada H, Hiraoka M: Tumor hypoxia: A target for selective cancer therapy. *Cancer Sci* 94:1021-1028, 2003.
73) Wang GL, Jiang BH, Rue EA, Semenza GL: Hypoxia-inducible factor 1 is a basic-helix-loop-helix-PAS heterodimer regulated by cellular O2 tension. *Proc Natl Acad Sci USA* 92:5510-5514, 1995.
74) Zhao M, Weissleder R: Intracellular cargo delivery using tat peptide and derivatives. *Med Res Rev* 24:1-12, 2004.
75) Dietz GP, Bahr M: Delivery of bioactive molecules into the cell: the Trojan horse approach. *Mol Cell Neurosci* 27:85-131, 2004.
76) Del Gaizo V, Payne RM: A novel TAT-mitochondrial signal sequence fusion protein is processed, stays in mitochondria, and crosses the placenta. *Mol Ther* 7:720-730, 2003.
77) Chen YN, Sharma SK, Ramsey TM, Jiang L, Martin MS, Baker K, Adams PD, Bair KW, Kaelin WG Jr: Selective killing of transformed cells by cyclin/cyclin-dependent kinase 2 antagonists. *Proc Natl Acad Sci USA* 96:4325-4329, 1999.
78) Pusztai L, Ayers M, Stec J, Clark E, Hess K, Stivers D, Damokosh A, Sneige N, Buchholz TA, Esteva FJ, Arun B, Cristofanilli M, Booser D, Rosales M, Valero V, Adams C, Hortobagyi GN, Symmans WF: Gene expression profiles obtained from fine-needle aspirations of breast cancer reliably identify routine prognostic markers and reveal large-scale molecular differences between estrogen-negative and estrogen-positive tumors. *Clin Cancer Res* 9:2406-2415, 2003.

79) Lipponen P: Apoptosis in breast cancer: relationship with other pathological parameters. *Endocr Relat Cancer* 6:13-16, 1999.
80) Lipponen PK, Aaltomaa S: Apoptosis in bladder cancer as related to standard prognostic factors and prognosis. *J Pathol* 173:333-339, 1994.
81) Lipponen P, Aaltomaa S, Kosma VM, Syrjanen K: Apoptosis in breast cancer as related to histopathological characteristics and prognosis. *Eur J Cancer* 30A:2068-2073, 1994.
82) Zhang GJ, Kimijima I, Abe R, Watanabe T, Kanno M, Hara K, Tsuchiya A: Apoptotic index correlates to bcl-2 and p53 protein expression, histological grade and prognosis in invasive breast cancers. *Anticancer Res* 18:1989-1998, 1998.
83) Martinez A, Walker RA, Shaw JA, Dearing SJ, Maher ER, Latif F: Chromosome 3p allele loss in early invasive breast cancer: detailed mapping and association with clinicopathological features. *Mol Pathol* 54:300-306, 2001.
84) Vaupel P, Schlenger K, Knoop C, Hockel M: Oxygenation of human tumors: evaluation of tissue oxygen distribution in breast cancers by computerized O2 tension measurements. *Cancer Res* 51:3316-3322, 1991.
85) Hohenberger P, Felgner C, Haensch W, Schlag PM: Tumor oxygenation correlates with molecular growth determinants in breast cancer. *Breast Cancer Res Treat* 48:97-106, 1998.
86) Bos R, Zhong H, Hanrahan CF, Mommers EC, Semenza GL, Pinedo HM, Abeloff MD, Simons JW, van Diest PJ, van der Wall E: Levels of hypoxia-inducible factor-1 alpha during breast carcinogenesis. *J Natl Cancer Inst* 93:309-314, 2001.

Diffusion-Tensor Fiber Tractography: Intraindividual Comparison of 3.0-T and 1.5-T MR Imaging[1]

Tsutomu Okada, MD
Yukio Miki, MD, PhD
Yasutaka Fushimi, MD
Takashi Hanakawa, MD, PhD
Mitsunori Kanagaki, MD, PhD
Akira Yamamoto, MD
Shin-ichi Urayama, PhD
Hidenao Fukuyama, MD, PhD
Masahiro Hiraoka, MD, PhD
Kaori Togashi, MD, PhD

Purpose: To prospectively evaluate the depiction of brain fiber tracts at 3.0- versus 1.5-T diffusion-tensor (DT) fiber tractography performed with parallel imaging.

Materials and Methods: Institutional review board approval was obtained, and each subject provided written informed consent. Subjects were 30 healthy volunteers (15 men, 15 women;. mean age, 28 years; age range, 21–46 years). Single-shot spin-echo echo-planar magnetic resonance (MR) sequences with parallel imaging were applied. Four fiber tracts were reconstructed: corticospinal tract (CST), superior longitudinal fasciculus (SLF), corpus callosum (CC), and fornix. Two neuroradiologists compared 3.0- and 1.5-T tractography in terms of fiber tract depiction by using five depiction scores (scores 0–4) and numbers of reconstructed tract fibers and in terms of lateral asymmetry in the CST by using numbers of reconstructed fibers. The Wilcoxon signed rank test was applied for statistical analysis.

Results: Visual scores for both CST hemispheres ($P < .001$), the right SLF ($P = .005$), the CC ($P = .01$), and the right fornix ($P = .04$) were higher at 3.0-T DT tractography. Larger numbers of CST (right, $P = .008$; left, $P < .001$), SLF (right, $P = .001$; left, $P = .02$), and fornix (bilaterally, $P = .02$) tract fibers were depicted at 3.0 T. The asymmetry index for the CST was lower ($P < .001$) at 3.0 T. Visual scores for the left SLF and the left fornix and numbers of CC tract fibers were not significantly different.

Conclusion: Depiction of most fiber tracts was improved at 3.0-T DT tractography compared with depiction at 1.5-T tractography.

[1] From the Department of Diagnostic Imaging and Nuclear Medicine (T.O., Y.M., Y.F., M.K., A.Y., K.T.) and Department of Therapeutic Radiology and Oncology (M.H.), Graduate School of Medicine, and Human Brain Research Center (T.H., S.U., H.F.), Kyoto University, 54 Kawahara-cho, Shogoin, Sakyo-ku, Kyoto-shi, Kyoto 606-8507, Japan. From the 2004 RSNA Annual Meeting. Received December 30, 2004; revision requested March 17, 2005; revision received May 4; final version accepted June 1. Supported in part by grants from the Ministry of Health, Labor and Welfare of Japan (k0800006-01) and the Ministry of Education Culture, Sports, Science and Technology of Japan (C)(15591270).

Diffusion-tensor (DT) imaging is a magnetic resonance (MR) imaging technique that is sensitive to the orientation of mobility in intravoxel water molecules (1,2). DT imaging reveals two specific characteristics: diffusion anisotropy and the directional distribution of water diffusivity. When water diffusion in a tissue is almost the same in all directions, the diffusion is considered to be isotropic and have lower anisotropy. Conversely, when water diffusion is restricted along a specific direction, the diffusion is considered to be anisotropic and have higher anisotropy. Brain white matter has high diffusion anisotropy because diffusion is faster when it is parallel to the fiber direction than when it is the same in all other directions (3,4).

DT images of the human brain can be reconstructed for visualization of the macroscopic three-dimensional fiber tract architecture by using a process known as fiber tractography, or the fiber-tracking technique (5–10). DT imaging and fiber tractography are powerful tools for studying cerebral white matter and have been applied clinically to assess brain tumors (11,12), diffuse axonal injury (13), pediatric brain development (14), and cerebral infarcts (15).

With recent advances in actively shielded 3.0-T magnets, the use of high-field-strength MR imaging in clinical settings has become practical (16,17). Parallel imaging techniques, such as simultaneous acquisition of spatial harmonics, or SMASH (18); sensitivity encoding (19); and auto-SMASH–based generalized autocalibrating partially parallel acquisition (20), also have improved with recent advances in MR imaging hardware. Owing to shortened echo train lengths and echo times, parallel imaging techniques can be used to reduce artifacts related to spin-echo echo-planar imaging. Some reports have described the performance of parallel imaging in spin-echo echo-planar DT imaging and fiber tractography at 1.5 or 3.0 T (9,10,21–24). However, to our knowledge, in no reports have the differences between 3.0- and 1.5-T spin-echo echo-planar DT fiber tractography with parallel imaging been compared. Thus, the purpose of our study was to prospectively evaluate the depiction of brain fiber tracts at 3.0-T versus 1.5-T DT fiber tractography performed with parallel imaging.

Materials and Methods

Study Subjects

The study population comprised 30 healthy volunteers (15 men, 15 women; mean age, 28 years; age range, 21–46 years) with no history of neurologic injury or psychiatric disease. All subjects were examined by one of the authors (T.H., with 14 years of experience as a neurologist), and no subjects had abnormal neurologic signs or symptoms. Institutional review board approval was obtained for this study, and each subject provided written informed consent.

Data Acquisition

All subjects underwent 3.0- and 1.5-T DT imaging, which was performed by using a whole-body 3.0-T MR unit (Trio; Siemens, Erlangen, Germany) with a 40 mT/m gradient and a 1.5-T MR unit (Symphony; Siemens) with a 30 mT/m gradient, on the same day. MR imaging at 3.0 T was performed by one author (T.O.), and MR imaging at 1.5 T was performed by another author (Y.F.), both of whom had 8 years of experience as neuroradiologists and 2 years of experience in DT imaging. The time delay between 3.0- and 1.5-T MR imaging was less than 1 hour for all subjects. Both MR units were equipped with integrated parallel acquisition capability and a receive-only eight-channel phased-array head coil. Both the 3.0-T and the 1.5-T DT imaging examinations involved the use of single-shot spin-echo echo-planar sequences and nearly identical parameters: 5200/79 (repetition time msec/echo time msec), a 220-mm field of view, a 128 × 128 matrix, 3-mm section thickness without intersection gaps (matrix size, 1.7 × 1.7 × 3.0 mm), and four repetitions.

The generalized autocalibrating partially parallel acquisition algorithm was applied for parallel imaging with use of a reduction factor of two, 24 additional autocalibrating phase-encoding steps in the center of k-space, and a 75% partial Fourier technique in the phase-encoding direction. Only the bandwidths differed: A bandwidth of 1502 Hz per pixel was used for 3.0-T imaging, and a bandwidth of 1056 Hz per pixel was used for 1.5-T imaging. Motion-probing gradients were applied along 12 noncolinear directions with a b factor of 700 sec/mm^2 after one non–diffusion-weighted image (b = 0 sec/mm^2) was obtained. A total of 40 sections encompassed the entire cerebral hemisphere and the brainstem. The imaging times for 3.0- and 1.5-T DT imaging were almost the same—about 7.5 minutes.

Data Processing

DT imaging data sets were transferred, in Digital Imaging and Communications in Medicine format, to a Windows personal computer (IBM, New York, NY) workstation. DtiStudio, version 1.02, software (H. Jiang, S. Mori, Department of Radiology, Johns Hopkins University, Baltimore, Md) was used for tensor calculations (6,10). All source images from the DT imaging data sets were visually inspected by one author (T.O.), and images with visually apparent artifacts due to bulk motion were removed. In our DT imaging data set, there was low eddy current–related

Published online before print
10.1148/radiol.2382042192

Radiology 2006; 238:668–678

Abbreviations:
DT = diffusion tensor
ROI = region of interest

Author contributions:
Guarantors of integrity of entire study, T.O., Y.M., K.T.; study concepts/study design or data acquisition or data analysis/interpretation, all authors; manuscript drafting or manuscript revision for important intellectual content, all authors; approval of final version of submitted manuscript, all authors; literature research, T.O., Y.M., Y.F., H.F., M.H., K.T.; clinical studies, T.O., Y.M., Y.F., T.H., M.K., A.Y., S.U., K.T.; statistical analysis, T.O., Y.M., M.K., A.Y., M.H., K.T.; and manuscript editing, all authors

Address correspondence to Y.M. (e-mail: *mikiy@kuhp.kyoto-u.ac.jp*).

Authors stated no financial relationship to disclose.

geometric distortion between images obtained in each motion-probing gradient direction (23,25), so postprocessing distortion correction was not applied for this data set. After calculating the six independent elements of the 3 × 3 tensor and diagonalization, three eigenvalues and three eigenvectors were obtained (1,3–5). The eigenvector associated with the largest eigenvalue was assumed to represent the intravoxel fiber orientation. The fractional anisotropy map and directional color-coded map were synthesized (Fig 1). Fiber orientations were assigned specific colors on the color-coded map, as follows: Red represented the right-to-left orientation; green, the anterior-to-posterior orientation; and blue, the superior-to-inferior orientation (26).

Fiber Tractography

The DtiStudio software was used to also perform fiber tractography on the basis of the fiber assignments derived by means of the continuous tracking method (6,9,10). With this software, tracking from all the pixels inside the brain (ie, with the brute force approach) was performed, and tracking results that penetrated the two manually segmented regions of interest (ROIs) on the basis of the known anatomic distributions of tracts were assigned to specific tracts (ie, with the two-ROI approach). Propagation in each fiber tract was terminated if a voxel with a fractional anisotropy value of less than 0.2 was reached or if the inner product of two consecutive vectors was greater than 0.75. These conditions prohibited the turning of angles larger than 41° during tracking (10).

Four fiber bundles—the corticospinal tract, the superior longitudinal fasciculus, the corticocortical connection fibers through the corpus callosum, and the limbic fibers through the fornix—were reconstructed by drawing specific ROIs according to the anatomic distributions of each fiber tract. ROI manipulations were performed by one neuroradiologist (A.Y.) with 3 years of experience performing tractography and 10 years of experience as a neuroradiologist. This author was blinded as to whether the images had been obtained by using 3.0 T or 1.5 T when he performed each ROI segmentation.

For corticospinal tract tractography, two ROIs were placed on transverse non–diffusion-weighted (b = 0 sec/mm^2) images (10,12,15) according to established anatomic landmarks: The first ROI was placed in the cerebral peduncle bilaterally, and the second ROI was placed in the precentral gyrus bilaterally (27) (Fig 2a).

The superior longitudinal fasciculus was reconstructed at tractography by placing two ROIs in the cerebral deep white matter on a coronal directional color-coded map. The superior longitudinal fasciculus was identified on the coronal color-coded map as a region where the fiber orientation was anterior to posterior (green), lateral to the corona radiata (26,28). An anterior ROI was placed in the plane passing through the reconstructed corticospinal tract, and a posterior ROI was placed in the plane passing through the rostral surface of the splenium of the corpus callosum, with both ROIs covering the green area representing the superior longitudinal fasciculus (Fig 2c). Some "noise" fibers that were apparently tracing the error course were then removed (10).

Corpus callosum tractography was performed by imaging the combination of four different callosal fiber bundles. The primary ROI was placed in the corpus callosum in the midsagittal plane (Fig 2d). To visualize different parts of the callosal fibers, secondary ROIs were placed in four regions: two ROIs on the coronal color-coded map and two ROIs on the transverse color-coded map (Fig 2e). Anterior callosal fibers, referred to as minor forceps, were reconstructed by placing the ROI covering the deep white matter in the coronal plane anterior to the genu of the corpus callosum. For reconstruction of the posterior cal-

Figure 1

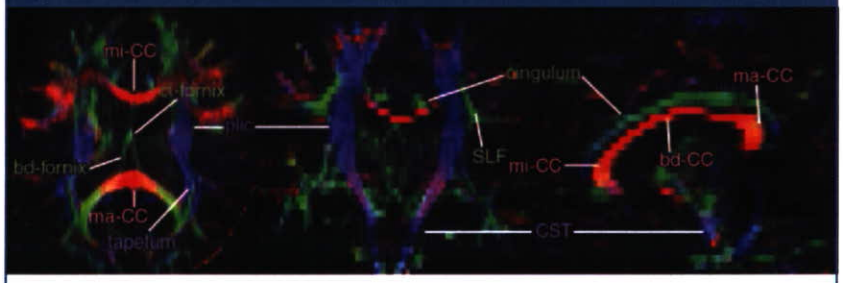

a.

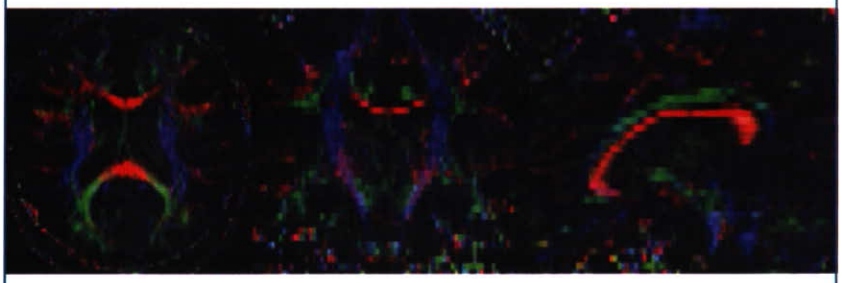

b.

Figure 1: Transverse (left), coronal (middle), and sagittal (right) **(a)** 3.0-T and **(b)** 1.5-T color-coded maps reconstructed at DT tractography in the same subject. Red, green, and blue areas represent fibers running in right-to-left, anterior-to-posterior, and superior-to-inferior orientations, respectively. Locations of examined white matter tracts were assigned by using the 3.0-T color-coded maps. *bd-CC* = body of corpus callosum, *bd-fornix* = body of fornix, *cl-fornix* = column of fornix, *CST* = corticospinal tract, *ma-CC* = major forceps, *mi-CC* = minor forceps, *plic* = posterior limb of internal capsule (including the corticospinal tract), *SLF* = superior longitudinal fasciculus.

Figure 2

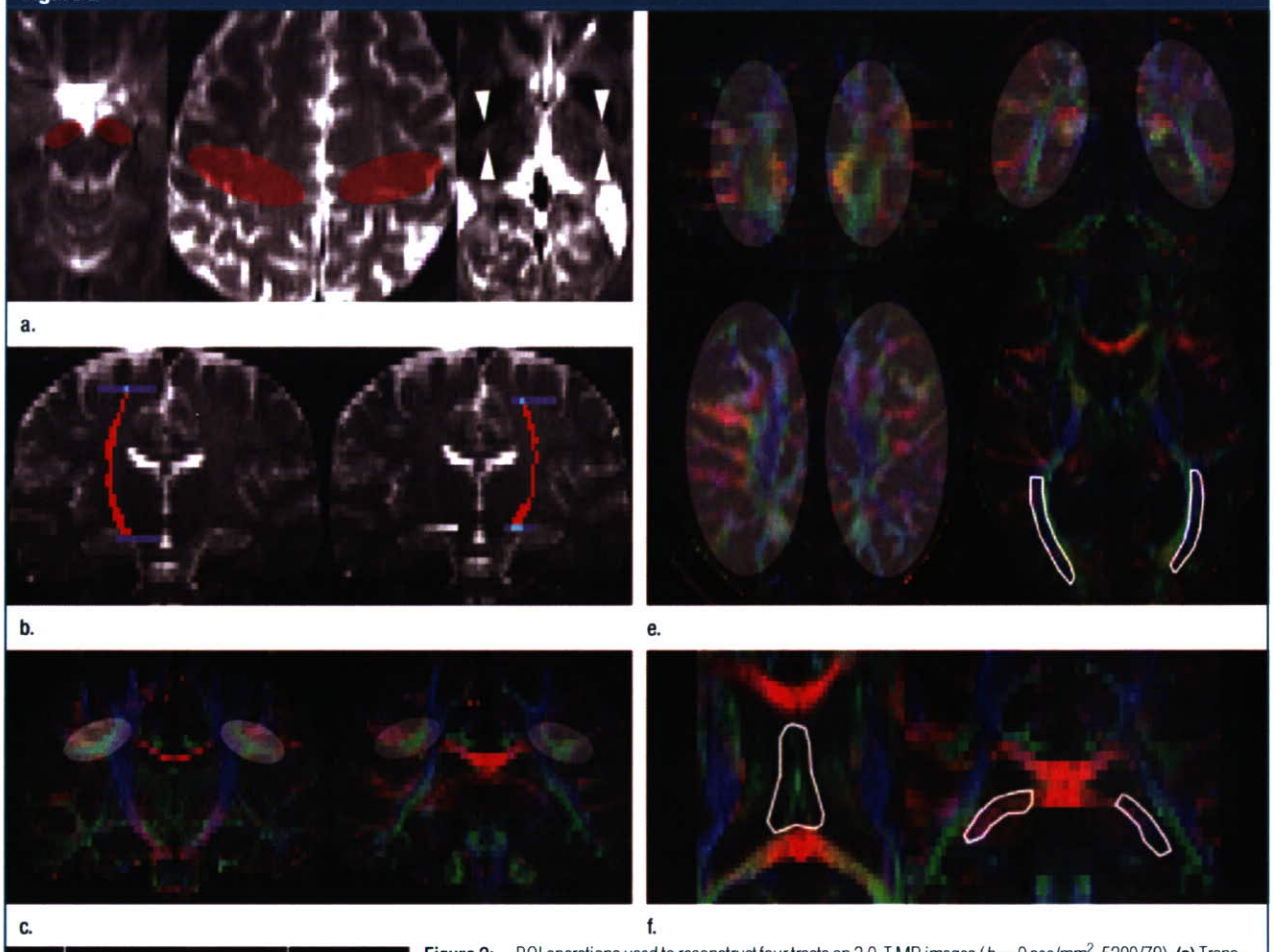

Figure 2: ROI operations used to reconstruct four tracts on 3.0-T MR images ($b = 0$ sec/mm^2, 5200/79). **(a)** Transverse images at bilateral cerebral peduncles (right), precentral gyri (middle), and internal capsule (left) show ROIs in red. Corticospinal tract is area of prolonged T2 relaxation at posterolateral aspect of internal capsule (arrowheads). **(b)** Coronal images of corticospinal tracts (red) reconstructed with cut operation. Only fibers between the ROIs (blue) were reconstructed for the right and left sides separately. **(c)** Coronal color-coded maps with ROIs (white ellipses). Anterior (left) and posterior (right) ROIs contain superior longitudinal fasciculus (green area lateral to corona radiata). **(d)** Primary ROI placed in corpus callosum on sagittal color-coded map. Vertical (coronal planes) and horizontal (transverse planes) white lines indicate section locations of secondary ROIs: anterior coronal section for minor forceps, posterior coronal for major forceps, superior transverse for body of corpus callosum, and inferior transverse for tapetum. **(e)** Transverse color-coded maps show secondary ROIs for corpus callosum: anterior ROIs for minor forceps (top left), posterior ROIs for major forceps (top right), superior ROIs for body of corpus callosum (bottom left), and inferior ROIs (white outlines) for tapetum (bottom right). **(f)** Transverse (left) and coronal (right) color-coded maps show ROIs (white outlines) for fornix. Primary (superior) ROI was placed at body of fornix (left); secondary (posterior) ROIs, at crura of fornices bilaterally (right).

losal fibers, referred to as major forceps, the ROI was placed posterior to the splenium of the corpus callosum. Callosal body fibers were reconstructed by placing the ROI at the centrum semiovale in the transverse plane superior to the body of the corpus callosum. For reconstruction of the temporal interhemispheric connection fibers, referred to as tapetum, ROIs were placed bilaterally in the temporal deep white matter, lateral to the trigon of the lateral ventricles. These four fibers (ie, minor forceps, major forceps, callosal body fibers, and tapetum) were combined to delineate the entire corpus callosum.

Limbic fibers through the fornix were reconstructed by placing one primary ROI and two secondary ROIs. The primary ROI was placed in the body of the fornix, and the secondary ROIs

Figure 3

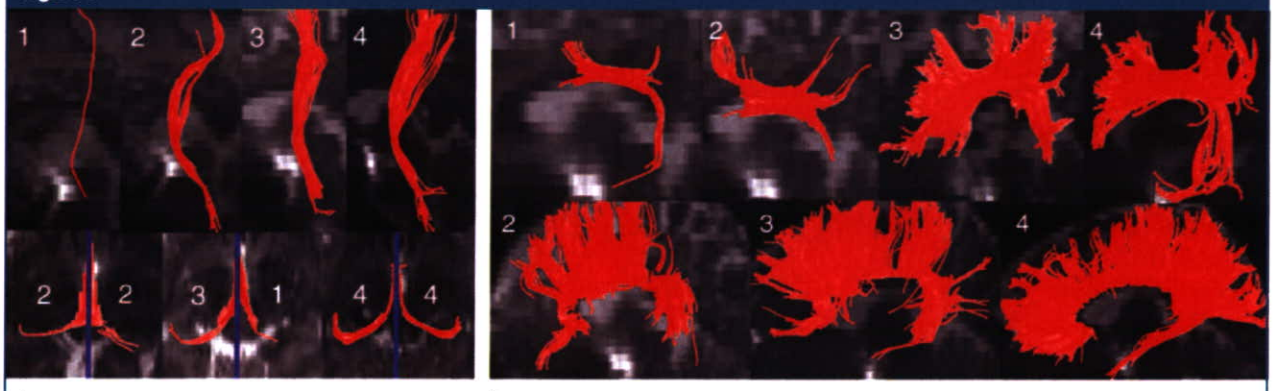

a. b.

Figure 3: Scoring (scores *1–4*) for fiber tract depiction at tractography. Red areas represent the depicted tracts. **(a)** Top: Corticospinal tractographic image superimposed on sagittal non–diffusion-weighted images (5200/79) viewed from left side. Grades *1* and *2* were assigned at 1.5-T imaging, and grades *3* and *4* were assigned at 3.0-T imaging. Bottom: Fornix tractographic image obtained at 3.0 T superimposed on transverse non–diffusion-weighted images (5200/79). Blue lines separate right and left fornix tractographic images. **(b)** Superior longitudinal fasciculus tractographic image (top) and corpus callosum tractographic image (bottom) superimposed on sagittal non–diffusion-weighted images (5200/79) viewed from left side. For superior longitudinal fasciculus tractography (top), grades 1 and 2 were assigned at 1.5-T imaging, and grades 3 and 4 were assigned at 3.0-T imaging. For corpus callosum tractography, grade 2 was assigned at 1.5 T imaging, and grades 3 and 4 were assigned at 3.0-T imaging. In no subject was grade 1 assigned at corpus callosum tractography.

were placed in the crura of the right and left fornices anterolateral to the splenium of the corpus callosum (Fig 2f).

Evaluation of Tractography

The tractographic depiction of fiber tracts was graded on three-dimensional volume views and in three orthogonal two-dimensional planes by two neuroradiologists (T.O., with 2 years of experience performing tractography; Y.M., with 3 years of experience performing tractography and 19 years of experience as a neuroradiologist). Grading was performed on the basis of the following three criteria: the fiber tract volume, the anatomic distribution of the tract, and the presence or absence of the tract at the expected location. The readers were blinded to the magnetic field strength used (1.5 or 3.0 T). After performing independent interpretations, the two readers resolved any score discrepancies by consensus to establish final scores.

One score was derived from one tractographic examination—not from the pair of ROIs used to perform reconstructing tractography. The scores assigned at fiber tractography were as follows: 4 meant excellent—that is, the depicted fiber tract accurately matched the known anatomic distribution, and there was a sufficient volume of fibers; 3 meant adequate for diagnosis—that is, imaging errors such as image distortion and tract propagation error were minor, so the image was still adequate for use as a diagnostic tool; 2 meant fair—that is, moderate imaging errors or moderate tract volume loss markedly reduced imaging quality; 1 meant poor—that is, there were major imaging errors and/or tract volume loss, and the readers were unable to interpret the course or shape of the tract; and 0 meant no tract visualization.

At corticospinal tract tractography, anatomically accurately depicted tracts were defined as those passing through the lateral segment of the cerebral peduncle, the posterior limb of the internal capsule, and the precentral gyrus. At superior longitudinal fasciculus tractography, fibers connecting the frontal and parietal lobes (ie, long association fibers) and fibers connecting the frontal and temporal lobes (ie, arcuate fibers) were considered. Anatomically accurate results for the superior longitudinal fasciculus were defined as good visualization of both the long association fibers and the arcuate fibers. At corpus callosum tractography, anatomically accurate results were defined as good visualization of the four different subsegments. At limbic tractography, the depiction of fibers connecting the column, body, and crus of the fornix was considered to represent anatomically accurate results. At tractography, the depicted superior longitudinal fasciculus, corpus callosum, and fornix are each composed of several subsegments of fiber bundles, and all subsegments were integrated to establish a single final score for each tractographic examination. The scoring of tractographic images is illustrated in Figure 3.

Tractographic depictions of the corticospinal tract, superior longitudinal fasciculus, and fornix on the right and left sides were assessed independently. At corpus callosum tractography, the right and left sides were assessed together, because callosal fiber connects the right and left hemispheres.

Reconstructed tract fibers were counted by using the DtiStudio software. The numbers of fibers depicted at tractography of the corticospinal tract and the superior longitudinal fasciculus in the right and left hemispheres were counted separately. The right and left fibers were not counted separately at tractography of the corpus callosum and

the fornix, because right- and left-hemisphere limbic fibers were difficult to differentiate at the column of the fornix, which was visualized as a single fiber bundle.

Although the diffusion characteristics of the normal brain are somewhat asymmetric, corticospinal tract tractography in healthy subjects reportedly reveals minimal asymmetry (17,29). To assess the reliability of corticospinal tract tractography in healthy subjects, lateral asymmetry was evaluated on the basis of the numbers of right- and left-hemisphere fibers at tractography of the corticospinal tract. For this purpose, the "cut" operation was performed by using DtiStudio software. With the cut operation, only the fiber coordinates between the two ROIs are reconstructed (Fig 2b). The conventional two-ROI approach involves the use of three corticospinal tract regions at tractography: the areas below the cerebral peduncle, between the two ROIs, and above the precentral gyrus. These three regions have very different properties. In the region between the two ROIs, tracking results do not branch and are more robust against noise. This approach is particularly useful for quantitative analysis.

The index of asymmetry (AI) between the right *(R)* and left *(L)* corticospinal tracts in each subject at tractography was calculated as the absolute difference in fiber numbers between the two sides, divided by the mean of the two sides, as modified from a previously described method (14): $AI = L - R / [(L + R)/2]$. Lateral asymmetry analysis of superior longitudinal fasciculus tractography was not performed, because the superior longitudinal fasciculus comprises numerous long and short connecting fibers and lateral asymmetry is commonly observed in healthy subjects (6,29).

Statistical Analyses

Differences between 3.0- and 1.5-T DT imaging were calculated in terms of the following features: *(a)* depiction scores for right and left corticospinal tract tractography, right and left superior longitudinal fasciculus tractography, corpus callosum tractography, and right and left fornix tractography; *(b)* numbers of fibers depicted at right and left tractography of the corticospinal tract, right and left tractography of the superior longitudinal fasciculus, corpus callosum tractography, and fornix tractography; and *(c)* asymmetry index at corticospinal tract tractography. Statistical

Figure 4

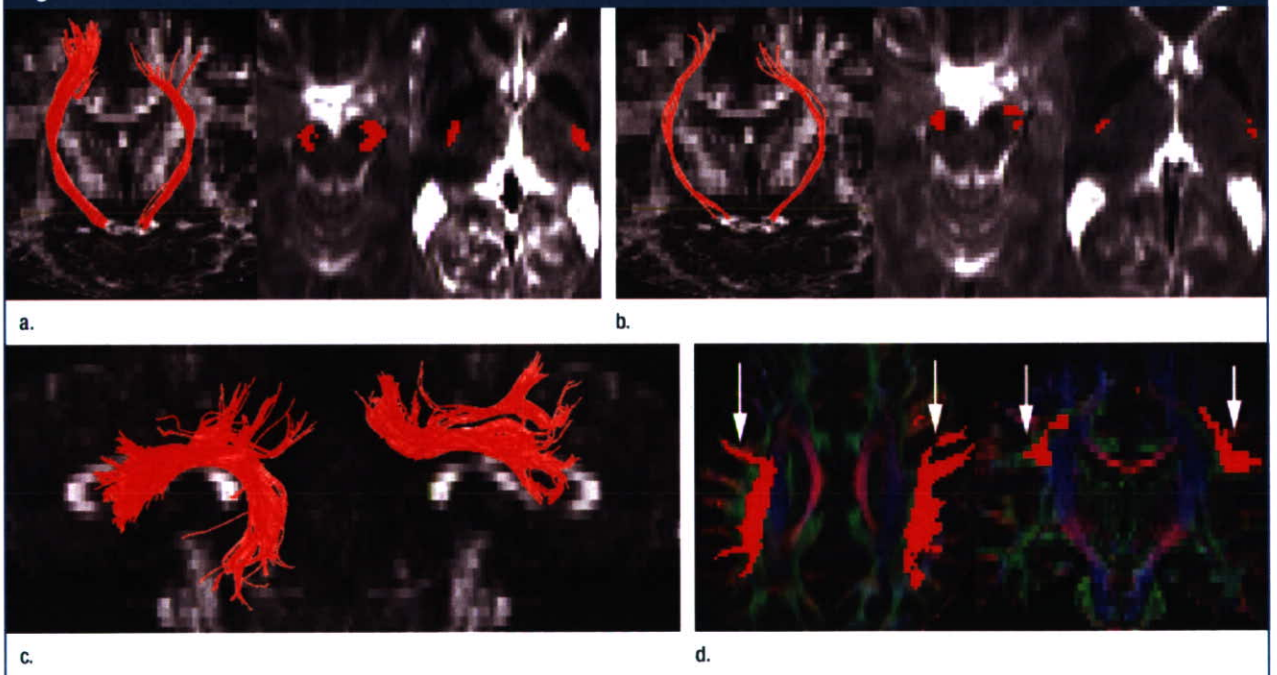

Figure 4: Fiber tractographic results. **(a, b)** Left: Three-dimensional reconstruction of corticospinal tract (red) in the same subject at **(a)** 3.0-T and **(b)** 1.5-T tractography, with use of transverse and coronal fractional anisotropy images. Middle and right: Transverse non–diffusion-weighted images with two-dimensional overlays of tractographic images at the sections of the cerebral peduncles (middle) and internal capsule (right) bilaterally. The voxels where the depicted corticospinal tract penetrates the transverse planes are shaded red. At 1.5-T corticospinal tract tractography (**b**), although the proper anatomic distribution is depicted, the tract volume is lower than that at 3.0 T. **(c)** Three-dimensional reconstruction of superior longitudinal fasciculus (red) on sagittal fractional anisotropy map at 3.0-T tractography in a different subject. At tractography in this subject, the shapes and distributions of the right and left superior longitudinal fasciculi differed. Although tractography of the left superior longitudinal fasciculus depicted arcuate fibers toward the temporal lobe, tractography of the right superior longitudinal fasciculus depicted no arcuate fibers. The corticocortical long connection fibers between the frontal and parietal lobes, however, were thicker on the right side than on the left side. **(d)** Tractographic image of superior longitudinal fasciculus (red, arrows) overlaid on 3.0-T transverse (left) and coronal (right) color-coded maps obtained in the subject described in **c** *(Fig 4 continues).*

analysis was based on the consensus scores for each tract in each subject derived by the two neuroradiologists. The Wilcoxon signed rank test was applied by using JMP, version 5.1, software (SAS Institute, Cary, NC). For all statistical analyses, $P < .05$ was considered to be indicative of a significant difference.

Results

Fiber Tract Visualization

DT imaging at both 3.0 and 1.5 T was successfully performed in all 30 subjects. The corticospinal tract was visualized at 3.0 and 1.5 T (Fig 4a, 4b) in all subjects. At superior longitudinal fasciculus tractography, long association fibers were visualized in all subjects at 3.0 and 1.5 T. Right arcuate fibers were visualized in 22 subjects (73%) at 3.0 T and in 20 subjects (67%) at 1.5 T, whereas left arcuate fibers were identified in 29 subjects (97%) at 3.0 and 1.5 T (Fig 4c, 4d).

All four subsegments of the corpus callosum were successfully visualized at 3.0 and 1.5 T (Fig 4e) in every subject. The body and column of the fornix were visualized at 3.0 and 1.5 T in every subject. The right crus of the fornix was visualized in 21 subjects (70%) at 3.0 T and in 18 subjects (60%) at 1.5 T. The left crus of the fornix was visualized in 27 subjects (90%) at 3.0 T and in 25 subjects (83%) at 1.5 T (Fig 4f). One subject was incidentally found to have cavum septum pellucidum and cavum vergae. The right and left columns of the fornix were visualized separately in this subject (Fig 4g).

All tractographic results were included in the analysis of tract depiction scores and numbers of depicted tract fibers. All tractographic results for the corticospinal tract were included for asymmetry analysis. With regard to the 420 depiction scores (30 subjects times seven tracts times two readers), there were discrepancies between the two independent readers regarding 152 scores (36%). The two readers discussed the discrepancy and established a final consensus score in each case. The depicted fiber tracts and the depiction scores are listed in Table 1.

Statistical Analyses

For tractography of the corticospinal tract, both right- and left-hemisphere depiction scores ($P < .001$) and numbers of tract fibers (right, $P = .008$; left, $P < .001$) were significantly higher at 3.0 T than at 1.5 T. The asymmetry index at corticospinal tract tractography was significantly lower at 3 T ($P < .001$). For tractography of the right su-

Figure 4

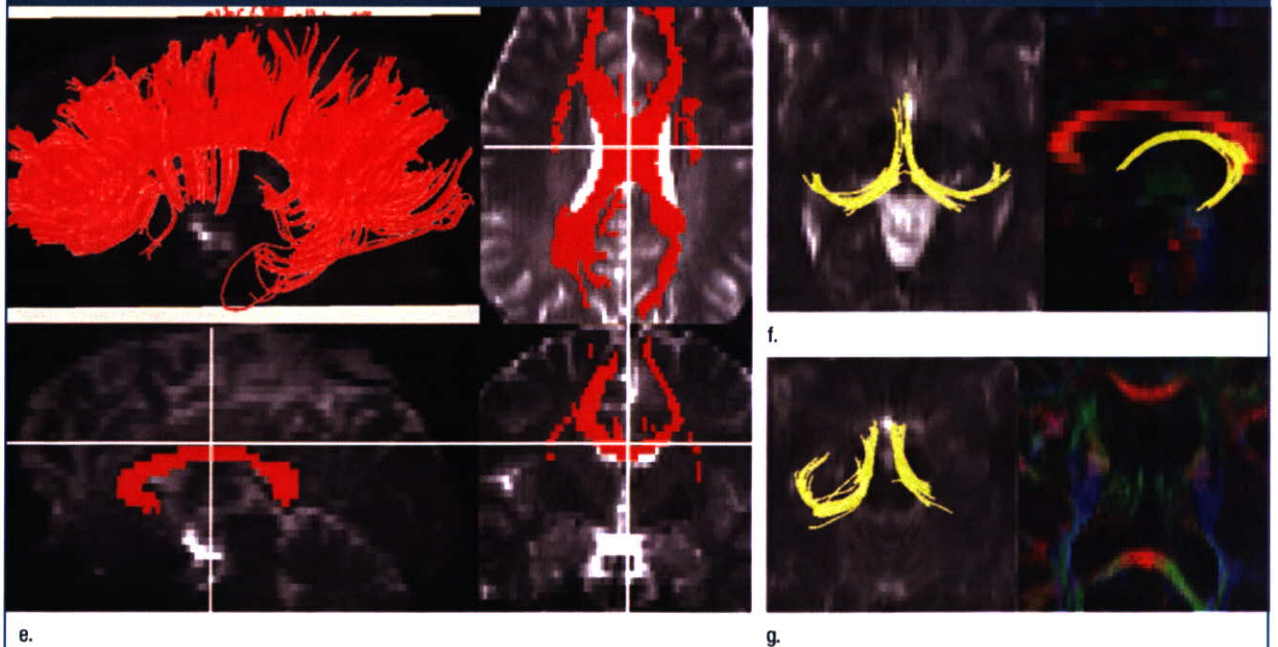

Figure 4 *(continued)*: **(e)** Three-dimensional 3.0-T tractographic reconstruction of corpus callosum (red) on sagittal non–diffusion-weighted image (5200/79) (top left) and on overlay in three orthogonal planes (top right, bottom left, and bottom right). Various kinds of transcallosal connection fibers are depicted. The center indicated by the intersecting of the vertical and horizontal lines on the three orthogonal images (top right, bottom left, and bottom right) indicate the same location. **(f)** Three-dimensional 3.0-T tractographic reconstruction of fornix (yellow) on transverse non–diffusion-weighted image (5200/79) (left) and sagittal color-coded map viewed from left (right). **(g)** Three-dimensional 3.0-T tractographic reconstruction of fornix (yellow) on transverse non–diffusion-weighted image (5200/79) (left) and transverse color-coded map (right) obtained in a subject with cavum septum pellucidum and cavum vergae. The bodies and columns of the fornices on the right and left sides were visualized separately.

perior longitudinal fasciculus, depiction scores (P = .005) and numbers of tract fibers (P = .001) were significantly higher at 3.0 T than at 1.5 T. Depiction scores for tractography of the left superior longitudinal fasciculus did not differ significantly between 3.0- and 1.5-T DT imaging. For tractography of the left superior longitudinal fasciculus, the numbers of tract fibers were significantly higher at 3.0 T than at 1.5 T (P = .02). For corpus callosum tractography, depiction scores were significantly higher at 3.0 T than at 1.5 T (P = .01), although the numbers of tract fibers did not differ significantly. Scores for depiction of the right fornix (P = .04) and numbers of fornix tract fibers bilaterally (P = .02) were significantly higher at 3.0 T than at 1.5 T, although scores for depiction of the left fornix were not significantly different. These results are summarized in Table 2.

Table 1

Depiction Scores Assigned at Fiber Tractography

Tract and Score	3.0-T Tractography	1.5-T Tractography
Right corticospinal tract		
0	0	0
1	0	2
2	1	8
3	6	13
4	23	7
Left corticospinal tract		
0	0	0
1	0	6
2	1	9
3	6	10
4	23	5
Right superior longitudinal fasciculus		
0	0	0
1	1	3
2	10	11
3	6	9
4	13	7
Left superior longitudinal fasciculus		
0	0	0
1	1	0
2	3	3
3	14	17
4	12	10
Corpus callosum		
0	0	0
1	0	0
2	2	6
3	9	14
4	19	10
Right fornix		
0	0	0
1	10	11
2	8	16
3	11	3
4	1	0
Left fornix		
0	0	0
1	3	4
2	14	17
3	12	9
4	1	0

Note.—Data are numbers of subjects with the given depiction score. Scores were determined in consensus between two readers.

Discussion

In recent studies, investigators have reported on intraindividual comparisons between 3.0- and 1.5-T DT imaging performed for functional MR imaging based on blood oxygen level–dependent contrast (30), intracranial time-of-flight MR angiography (31), supraaortic contrast material–enhanced MR angiography (32), and high-spatial-resolution inner ear imaging (33). These studies revealed the clinical feasibility of and the better visualization that is achievable at 3.0-T imaging compared with these features at 1.5-T imaging. DT imaging also reportedly yields a higher signal-to-noise ratio at 3.0 T, suggesting the possibility that it renders higher spatial resolution without enhanced noise-related errors (22,34).

Parallel imaging techniques involve the use of multiple receiver coil elements for spatial information encoding and gradient encoding and, owing to shortened echo train lengths, have been shown to markedly reduce the number of echo-planar imaging–related artifacts. The potential of parallel imaging for DT imaging has been demonstrated at both 1.5 and 3.0 T (21,22). Naganawa et al (23) challenged the optimization of 3.0-T DT fiber tractography performed with parallel imaging and found that DT imaging data on brain fiber tracking in healthy subjects can be acquired within a very short imaging time (<2 minutes). Nagae-Poetscher et al (24) performed high-spatial-resolution DT imaging of the brainstem at 3.0 T with parallel imaging and visualized various brainstem structures, including deep cerebellar nuclei, some cranial nerves, and white matter tracts.

To our knowledge, our study is the first in which the findings of 3.0- and

1.5-T DT fiber tractography, both performed with parallel imaging, were compared in a relatively large number of subjects. Improved image quality was observed at 3.0-T tractography of the corticospinal tract.

More complex results were observed at tractography of the superior longitudinal fasciculus. Although the right superior longitudinal fasciculus was visualized significantly better at 3.0 T, the depiction score for left superior longitudinal fasciculus tractography did not differ significantly between 3.0 and 1.5 T. The numbers of tract fibers depicted at 3.0 T were significantly higher than the numbers of fibers depicted at 1.0 T. We speculated that the reason for this was as follows: According to fiber dissection study findings, the corticospinal tract is a long projection fiber bundle with a well-established anatomic distribution (35). Most fibers in the corticospinal tract run parallel through the posterior limb of the internal capsule, without sharp turning angles or directional diversity.

Conversely, both the superior longitudinal fasciculus and the corpus callosum consist of groups of fiber bundles that comprise association or commissural fibers of varying lengths and directions. The superior longitudinal fasciculus contains arcuate fibers that turn sharply toward the temporal lobe. This sharp turning angle may surpass the tracking terminate threshold, and tracking does not extend to reach the temporal lobe. Temporal fibers are susceptible to image distortion at the middle cranial fossa and temporal bone, where the air-tissue interface induces magnet susceptibility artifacts. Thus, we propose that temporal arcuate fibers are more affected by image distortion than are long association fibers. In the present study, left arcuate fibers were visualized in a larger number of subjects than were right arcuate fibers at both 3.0 and 1.5 T. Such asymmetry of the arcuate fibers at tractography may be due to image distortion or the known lateral asymmetry of temporal fibers (36), and, thus, differences between 3.0- and 1.5-T DT imaging may be underestimated on the left side.

Table 2

Analyses of Tract Depiction Scores and Numbers of Tract Fibers

Tract	Difference in Depiction Score*	*P* Value†	Difference in No. of Tract Fibers*	*P* Value‡
Right corticospinal tract§	0.87 ± 0.15	<.001	27 ± 12	.008
Left corticospinal tract	1.32 ± 0.21	<.001	70 ± 9.2	<.001
Right superior longitudinal fasciculus	0.52 ± 0.16	.005	192 ± 57	.001
Left superior longitudinal fasciculus	0.03 ± 0.14	NS	65 ± 34	.02
Corpus callosum	0.34 ± 0.12	.01	220 ± 149	NS
Right fornix	0.35 ± 0.16	.04	...	...
Left fornix	0.19 ± 0.15	NS	...	...
Left and right fornices	...	...	14 ± 5.5	.02

Note.—NS = not significant.

* Data are mean difference values ± standard deviations.

† *P* values for difference in depiction scores at 1.5- versus 3.0-T tractography.

‡ *P* values for difference in numbers of tract fibers at 1.5- versus 3.0-T tractography.

§ The mean asymmetry index for the corticospinal tract was 0.47 ± 0.11 (standard deviation), and the difference in corticospinal tract asymmetry index at 1.5- versus 3.0-T tractography was significant ($P < .001$).

For corpus callosum tractography, tract depiction scores were better at 3.0 T than at 1.5 T but the numbers of tract fibers did not differ significantly. At corpus callosum tractography, the crossing-fiber problem of unidirectional tracking models (37) may contribute to the discrepancies observed between depiction scores and tract fiber numbers. Corpus callosum tractography is susceptible to the crossing-fiber problem at the centrum semiovale. In this area, a small number of callosal fibers intersect a large number of corticospinal tract fibers. Thus, corpus callosum tractography might reveal a smaller number of fibers than the appropriate fiber trajectory owing to limitations related to the crossing-fiber problem, and differences between 3.0- and 1.5-T imaging may be underestimated.

The statistical methods used may have been responsible for the differences in results obtained at analyses of the depiction scores and the numbers of tract fibers. Although mean differences in the numbers of depicted fibers between 3.0- and 1.5-T imaging were as large as 220, no significant difference was noted. This was probably because of the relatively large numbers of depicted fibers (mean numbers: 3784 at 3.0 T and 3565 at 1.5 T). Low statistical power also may have contributed to this lack of a significant difference.

Depiction scores for right fornix tractography were significantly better at 3.0 T than at 1.5 T, but no significant differences were noted for the left fornix. The numbers of tract fibers depicted at 3.0-T fornix tractography were significantly higher than the numbers depicted at 1.5-T tractography. This result was probably due to the relatively lower volume of limbic fibers compared with the volumes of other fiber bundles. Our DT imaging voxel size was 1.7 × 1.7 × 3.0 mm. The body and crus of the fornix are composed of narrow fiber bundles—they are smaller in diameter than a single voxel—so partial volume-averaging artifacts would have had a greater effect in this region than in the other fiber tracts.

The present study had some limitations. First, the imaging parameters for 3.0-T imaging were not optimized to achieve the best DT image quality. For the most part, we used identical imaging parameters to perform 3.0- and 1.5-T imaging for comparisons so that features other than magnetic field strength would be equivalent. However, differences in T1 and T2* interfere with the equal conditions between 3.0- and 1.5-T imaging. A DT imaging sequence optimized for 1.5-T imaging is not the optimal sequence for 3.0-T imaging. The differences in bandwidth between 3.0- and 1.5-T imaging also may have biased